CrystEngComm

Accepted Manuscript

ROYAL SOCIETY OF CHEMISTRY

www.rsc.org/crystengcomm

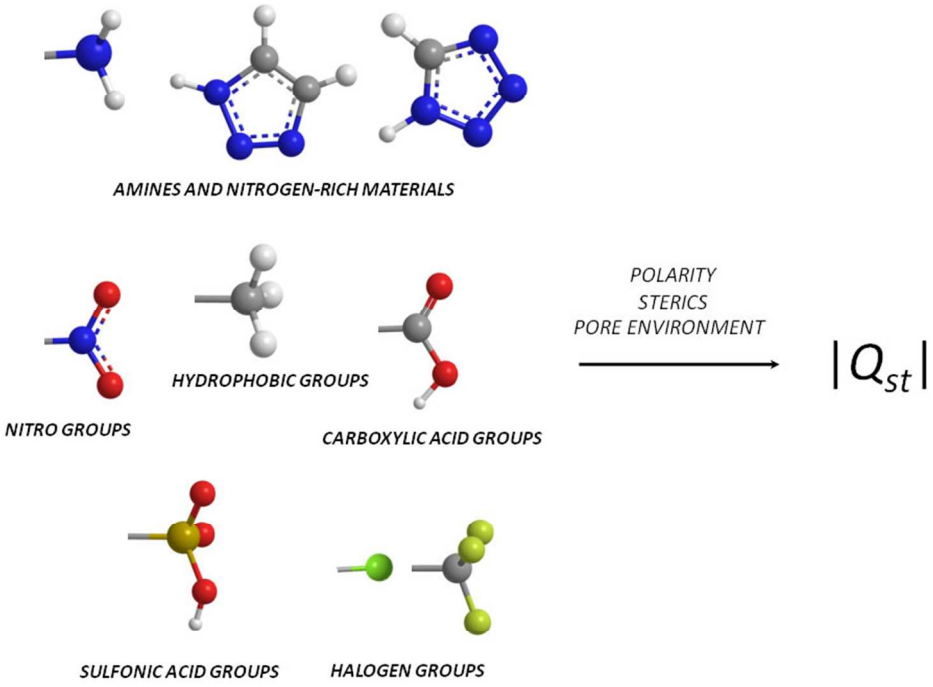

254x190mm (96 x 96 DPI)

Textural abstract

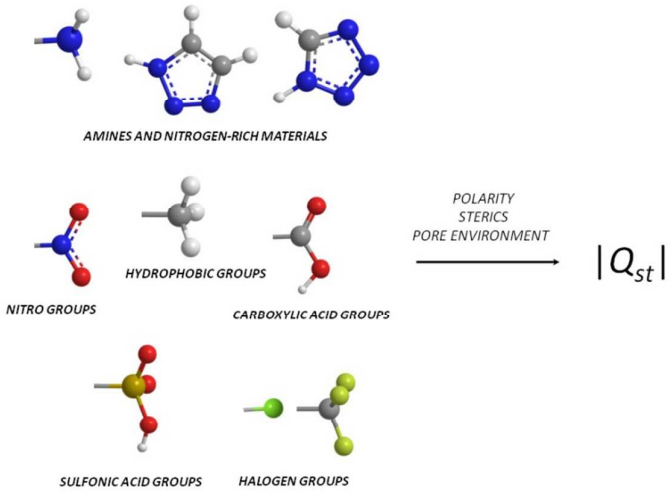

Tuning the functional sites in Metal-Organic Frameworks provides one strategy to vary the CO_2 adsorption properties – this highlight article provides insight into modulation of another key performance criterion, namely the isosteric heat of adsorption, and its influence on CO_2 capture.

Journal Name

RSCPublishing

ARTICLE

Tuning the Functional Sites in Metal-Organic Frameworks to Modulate CO_2 Heats of Adsorption

Cite this: DOI: 10.1039/x0xx00000x

Anita Das,[a] Deanna M. D'Alessandro[a*]

Received ooth January 2012,
Accepted ooth January 2012

DOI: 10.1039/x0xx00000x

www.rsc.org/

Metal-organic frameworks (MOFs) have been targeted as solid state sorbents for postcombustion carbon dioxide capture due, in part, to the enormous tunability of their structures through the incorporation of different functional sites. The isosteric heat of adsorption (Q_{st}) provides one measure of the interaction of a solid sorbent with guest molecules, and has a bearing on the low pressure (<1 bar) CO_2 uptake, selectivity and regenerability of a material. It is a key factor in the design of adsorbents for gas separation; however, it is sometimes overlooked in the evaluation of MOFs for CO_2 capture. This highlight article draws together the impact of various functional sites on the CO_2 heat of adsorption, and examines the interplay between functional sites and other factors such as competing water adsorption that influence a material's suitability for CO_2 capture from industrial streams.

Introduction

Metal-organic frameworks (MOFs) have garnered much attention for carbon dioxide (CO_2) capture and separation processes including postcombustion capture from power plant flue gas, precombustion separation, natural gas 'sweetening', and direct air capture, amongst others. Several recent reviews on the subject[1-6] have focussed on the CO_2 uptake and selectivity of MOFs at relevant partial pressures for a given separation process. The isosteric heat of adsorption for CO_2 represents a third key parameter of these materials that governs their performance under industrially-relevant conditions, as it determines the extent of the adsorbent temperature changes during the adsorption (exothermic) and desorption (endothermic) processes.[7] The isosteric heat of adsorption (Q_{st}) is a thermodynamic quantity defined as the negative differential change in total enthalpy (ΔH_{ads}) of a closed system. It is by definition a positive quantity, while the (exothermic) enthalpy of adsorption is a negative quantity (Equation 1). It is typical to report the two values in the same way; and for the purposes of this article, "increasing heat of adsorption" refers to an increase in the magnitude of the isosteric heat of adsorption which will herein be referred to as $|Q_{st}|$. For CO_2 capture applications in which the material undergoes multiple adsorption-desorption cycles, this parameter has an important bearing on the low pressure (<1 bar) CO_2 uptake, selectivity and regenerability of a material. In the latter case, a minimal energy penalty for regeneration is key. The importance of this parameter (among other key metrics in the consideration of MOFs for CO_2 capture materials) is highlighted in a recent review by Bae and Snurr.[8] For postcombustion capture applications in particular, this regeneration energy represents a major contribution to the cost of the overall process which, using current amine-based wet-scrubbing methods, contributes to the 25-40% energy penalty.[1]

Towards the goal of improving the efficiency of separation processes such as postcombustion capture, MOFs offer a potentially viable technology with enormous potential for tunability of their chemical and physical properties. An important strategy in the development of MOFs for CO_2 capture has involved the inclusion of specific functional sites to improve the uptake, selectivity and heat of adsorption.

In reality, a trade-off exists between these fundamental properties, and the selection of an optimal material for a given separation requires consideration of a number of variables that impact the performance of a material under industrially-relevant conditions, including the stability, processability and potential for scale-up amongst other factors. It is also important to note that industrial flue streams contain a variety of other components, including water vapour that necessarily impact the CO_2 uptake, selectivity and heat of adsorption. Experimental measurements in mixed-streams are particularly challenging, and as a result, computational methods such as Ideal Adsorbed Solution Theory (IAST)[9] have been employed to simulate materials' performance under more realistic conditions. With the design and synthesis of an ever-increasing number of novel organic ligands to improve MOF performance in CO_2 capture applications, this highlight article draws together the literature to-date in the field of postcombustion CO_2 capture to explore the impact of functional sites on the isosteric heat of adsorption, $|Q_{st}|$.

In chemically functionalised frameworks, the magnitude of $|Q_{st}|$ is often employed as a measure of the host-guest interaction. In general, a higher magnitude of $|Q_{st}|$ corresponds to an improved selectivity for CO_2 over other components of a mixed gas stream (specifically, CO_2/N_2 and CO_2/CH_4). The magnitude of $|Q_{st}|$ is often used to infer the nature of the CO_2-framework interaction, with values under 30 kJ/mol generally indicative of physisorption interactions, values of 30–50 kJ/mol indicative of moderately strong interactions, and values above 50 indicative

of strong interactions, nearing the magnitude of a chemisorption interaction. For postcombustion capture, the desired range for the heat of adsorption is believed to lie between the physisorption and chemisorption regimes, which is optimal for regenerability of a material with sufficient CO_2 specificity.

The $|Q_{st}|$ data reported in this review represent measurements from pure gas adsorption isotherms. Calculations of $|Q_{st}|$ are typically derived from isotherm data obtained at two or three temperatures. The most straightforward derivation is arrived at through modelling the data according to the Clausius-Clapeyron equation (Equation 1). Virial expansions and spline functions can be employed to determine pressure as a function of uptake in order to plot adsorption isosteres (ln P as a function of 1/T) such that Equation 1 may be applied; however in each case, the $|Q_{st}|$ value obtained is only as accurate as the fit itself. The Clausius-Clapeyron equation assumes (i) the ideality of the gas at standard conditions, (ii) a constant enthalpy over the temperature range of interest (though this is never strictly true, the assumption holds well at moderate pressures) and (iii) the vapour pressure is 1 atm. Notably, several of these assumptions are invalid at high pressures and near the critical point of the substance being measured; under these conditions, the Clausius-Clapeyron relation will give inaccurate results. The related quantity, differential heat of adsorption (Q_d), can be measured using differential scanning calorimetry (DSC) methods, although this is less common.[10]

$$Q_{st} = -\Delta H_{ads} = -R\left(\frac{d\ln P}{d\left(\frac{1}{T}\right)}\right) > 0$$

Equation 1. The Clausius-Clapeyron equation

The incorporation of specific functional sites that interact selectively with CO_2 over other components of a mixed gas stream represents one key strategy towards optimising the selectivity and heat of adsorption. Some examples of such sites include open metal centres, amines (alkyl/aryl), *N*-heterocycles, sulfonic acids, carboxylic acids, sulfones, hydroxyl groups, nitro groups, halogen groups and ionic species in the pore. By and large, such interaction is inferred by an increase in the magnitude of $|Q_{st}|$ for CO_2 relative to an unfunctionalised framework equivalent, with several papers also providing accompanying computational work and more direct experimental evidence of CO_2-host interactions via *in situ* spectroscopic or crystallographic techniques. Different framework topologies with identical functional groups can show a large degree of variability of interaction (particularly in heat of adsorption at non-zero coverage), and the mechanism of interaction with these functional groups is seldom examined in detail (although cases of *in situ* gas dosing with X-ray diffraction/neutron diffraction/infrared spectroscopy are becoming increasingly common).[11] Additionally, other factors impacting CO_2-host interactions (e.g., pore/aperture size, accessibility of functional group) are often neglected in the discussion of functionalised frameworks.

This highlight focuses on a comparison of $|Q_{st}|$ values and their relationship with specific binding sites in MOFs for CO_2 capture published in the literature. This article also seeks to identify other factors contributing to CO_2 uptake and selectivity which are sometimes overlooked in the discussion of frameworks containing CO_2 binding sites. In doing so, we hope to clarify the factors that must be considered in the selection of appropriate functional sites. For reference, a comprehensive list of frameworks and associated heats of adsorption are listed in Table 1. A list of ligands is also provided for ease of reference.

A Open Metal Sites

Copper paddlewheel frameworks

Coordinatively unsaturated metal centres have been extensively explored as binding sites for guests (particularly H_2 and CO_2) in MOFs. One of the archetypal frameworks is $[Cu_3(btc)_2]$ (HKUST-1),[12] which has been shown to have a strong preference for CO_2 over N_2, and has a $|Q_{st}|$ at low coverage of 30 kJ/mol,[13] consistent with a moderately strong end-on interaction between the CO_2 molecule and the metal centre $[O{=}C{=}O\cdots Cu^{2+}]$ which has been characterised by *in situ* infrared spectroscopic studies.[14] Interestingly, when water is bound to the open Cu^{2+} sites in the hydrated framework, the CO_2 uptake at low pressure was improved, and the heat of adsorption was slightly increased.[15] A plethora of other Cu^{2+} paddlewheel-based frameworks have been reported in the literature for CO_2 capture applications,[16-20] but relatively few of these publications have reported heat of adsorption data to indicate the strength of interaction with the open Cu^{2+} sites. In one of the few examples, the framework $[Cu_4(mttbpdc)]$ (NOTT-140, Figure 1) exhibited an heat of adsorption of 24.7 kJ/mol.[21] The lower heat of adsorption compared to $Cu_3(btc)_2$ may be attributed to a larger Jahn-Teller effect resulting in an elongation of the $Cu^{2+}\cdots O$ interaction.

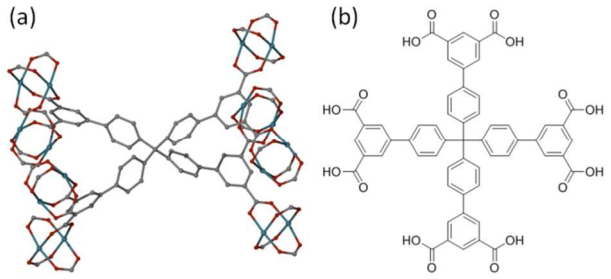

Figure 1. (a) The connectivity of $mttbpdc^{8-}$ to eight $[Cu_2(O_2CR)_4]$ paddlewheel units and (b) the $H_8mttbpdc$ ligand

Activation of these materials is particularly important due to the ease with which the open metal sites may be "poisoned" (e.g., with humidity/water). This was highlighted in a study by Kim *et al*. in which Cu^{2+} paddlewheels were synthesised with the ligand H_4tcm. Activation of the framework via heating resulted in a $|Q_{st}|$ of 29.7 kJ/mol, whereas supercritical CO_2 activation resulted in a value of 36.1 kJ/mol, as well as a higher overall uptake up to 1 bar.[22]

The coordination environment of a coordinatively unsaturated metal centre will also influence its strength as a Lewis acid interaction site for CO_2. This was observed in the benzenetristriazolate framework CuBTTri ($H_3[(Cu_4Cl)_3(BTTri)_8]$) which has N-donors bound to the Cu^{2+}

centre, rather than O-donors seen in most frameworks containing open Cu^{2+} centres (e.g., copper paddlewheel motif in $[Cu_3(btc)_2]$ and NOTT-140; $[Cu_2(dobdc)]$, *vide infra*). This results in a low heat of adsorption (21 kJ/mol) which is only marginally higher than that for self-condensation of CO_2 (17 kJ/mol) resulting from the difference in electronic structure around the metal centre.[23] Zhang and coworkers investigated an isotypic sodalite framework incorporating btc^{3-} (i.e., an analogous ligand with O-donors instead of N-donors, $X_3[(Cu_4Cl)_3(btc)_8]$ where X = tetramethyl ammonium, tetraethylammonium or tetrapropylammonium) exhibits higher heats of adsorption in the range 25.3-27.3 kJ/mol compared to CuBTTri; however, it was not possible to discern whether the coordination environment around the open Cu^{2+} centre or the charged framework surface contributed to a greater extent to the higher magnitude of $|Q_{st}|$. Variation of the counterion also brings to light interesting pore size effects in this system, such that an optimal heat of adsorption was achieved when the tetramethylammonium counterion was occluded in the pore (Table 1).[24]

$[M_2(dobdc)]$ series (CPO-27-M, MOF-74)

The $[M_2(dobdc)]$ series (where M = Ni, Co, Zn, Mg, Mn, Cu, Fe; also known as the CPO-27 and MOF-74 series) has been of particular interest due to the ability to vary the identity of the open metal site within an isotopic series of frameworks. The variation of $|Q_{st}|$ with the identity of the open metal centre is particularly noteworthy; the significantly higher $|Q_{st}|$ of the magnesium analogue (47 kJ/mol, compared to 41 and 37 kJ/mol for the Ni and Co analogues, respectively) has been attributed to the strong ionic character of the end-on $Mg^{2+}\cdots O$ interaction.[25] This interaction has been supported by *in situ* ^{13}C NMR experiments as well as DFT and molecular dynamics simulations.[26] Additionally, in breakthrough experiments, $[Mg_2(dobdc)]$ was found to perform well when compared to commercial sorbents (e.g., methanolamine, MEA) and exhibited a favourable balance between dynamic capacity (dependent on the kinetics of diffusion through the pore) and energies of regeneration.[27] In a systematic study conducted by Long and coworkers in which $[Mg_2(dobdc)]$ was investigated as a candidate sorbent for CO_2/H_2 separations alongside high surface area frameworks, materials with strongly adsorbing sites were found to be superior candidates for Pressure Swing Adsorption (PSA) processes than higher surface area materials lacking such sites.[28] Similarly, in Temperature Swing Adsorption (TSA) breakthrough simulations carried out by the same group, $[Mg_2(dobdc)]$ was found to perform better at higher temperatures, with longer breakthrough times and good working capacity. This behaviour is directly related to the temperature dependence of the CO_2 isotherms, and improves with the strength of the sorption sites. The usefulness of a material for CO_2 capture from mixed streams was therefore found to be improved by the presence of strong sorption sites.[29] $[Ni_2(dobdc)]$ has also performed well in similar breakthrough experiments,[30] and has been found to out-perform the magnesium analogue under humid conditions (an important issue that is often neglected in the study of these materials).[31] Through *in situ* single crystal X-ray diffraction and infrared spectroscopy experiments, an "end-on" binding mode of CO_2 onto the Ni^{2+} open metal sites was elucidated, providing a mechanism for the moderately high CO_2 sorption capacity at sub-atmospheric pressures and ambient temperatures (Figure 2).[32] The relatively low enthalpy of interaction for the copper analogue ($|Q_{st}|$ = 24 kJ/mol) has been attributed to the Jahn-Teller effect resulting in an elongation of the M···O interaction distance as compared to the other congeners in the series.[33] It may be postulated that the order for CO_2 binding strengths in transition metal $[M_2(dobdc)]$ materials can be explained by the "effective" charge of the metal ions caused by the differences in 3*d* electron screening to the nucleus (i.e., CO_2 binding strength follows the Irving-Williams series such that the binding strength increases in the order Zn < Mn < Fe < Co < Ni; the copper analogue is a notable exception to this trend with a significantly lower $|Q_{st}|$ value due to the above mentioned Jahn-Teller effect).[34,35]

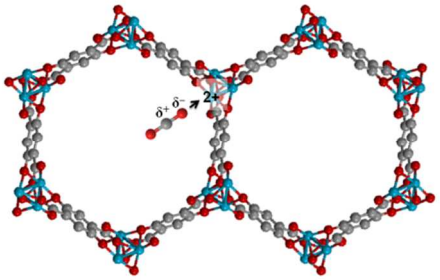

Figure 2. Schematic diagram showing the "end-on" CO_2 binding mode observed in $[Ni_2(dobdc)]$.

$[Mg_2(dobpdc)]$ which is topologically identical to the series discussed above, but with the ligand extended by one phenyl ring, gives a $|Q_{st}|$ of 44 kJ/mol – comparable to that of $[Mg_2(dobdc)]$ – indicating an absence of pore size effects in this case, with the low coverage value being entirely attributed to the interaction of CO_2 with the unsaturated Mg^{2+} site.[10] This is supported by solid-state NMR studies in this material with $^{13}CO_2$. These types of comparisons are interesting from the point of view examining the influence of pore size, as limited examples of such systematic studies exist. This is particularly true of frameworks with an "active" functional site for CO_2.

Vacancy Prussian blue analogues

Vacancy Prussian Blue Analogues (PBAs) provide a simple platform from which to study the effect of open metal sites. Thallapally *et al*. undertook a study measuring the CO_2 uptake and heat of adsorption in five PBAs, $M_3[Co(CN)_6]_2$ (M = Cu, Ni, Mn, Co, Zn).[36,37] The interaction was found to increase with metal substitution in the order Zn ~ Co < Cu < Ni < Mn (29, 29, 49, 54 and 67 kJ/mol, respectively). The higher heat of adsorption in the Cu, Ni and Mn analogues was also reflected in their increased low pressure uptakes. The Irving-Williams series does not hold in this case; this may be related to the stronger back-bonding effects of the cyanido ligands which negate the usual electrostatic effects responsible for the Irving-Williams series. The high crystallographic symmetry of such materials also facilitates the location of CO_2 molecules in the pore space by diffraction techniques.

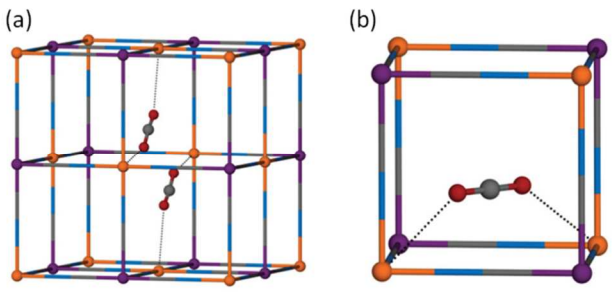

Figure 2. (a) CO_2 adsorption site located in a vacancy-type Prussian blue derivative, allowing the CO_2 to bridge between two Fe^{2+} bare metal sites. (b) CO_2 adsorption site located above the non-vacancy square faces of the framework showing the interaction with two Fe^{2+} centres. Reproduced from Ref. 38 with permission from The Royal Society of Chemistry.

Using *in situ* powder neutron diffraction, a unique "bridged" CO_2 molecule between two open metal sites was located as one of two binding sites in the Prussian blue analogue $Fe_3[Co(CN)_6]_2$ (the other site being defined as CO_2 interacting in a face capping motif) (Figure 2). This observation highlights the possibility of cooperative effects between multiple binding sites in a single pore space, one which is often disregarded in the analysis of such materials as it is quite often assumed to be a 1:1 CO_2:binding site ratio.[38]

Trivalent open metal sites

MIL-100 $[Cr_3F(H_2O)_3O(btc)_2]$ and MIL-101 $[Cr_3F(H_2O)_2O(bdc)_3]$ contain open Cr^{3+} sites and exhibit high enthalpies of adsorption, which have been shown by *in situ* IR and CO_2 dosing experiments to be the result of a strong end-on interaction with the coordinatively unsaturated Lewis acidic sites ($O{=}C{=}O\cdots Cr^{3+}$). The absence of IR bands suggested the chemical formation of a carbonate species in the sorption process. The stronger interaction of MIL-100 compared to MIL-101 (63 compared to 44 kJ/mol, respectively) was attributed to the lower acidity of the Cr^{3+} sites in the former as a result of extra-framework terephthalic acid impurities persisting inside the pores even after activation. The rapid decrease in $-|Q_{st}|$ in both cases suggested an initial strong adsorption onto the metal centre, followed by filling of the residual pore space which was characterised by relatively weaker interactions.[39]
Other open metal sites of high charge such as Al^{3+} have also been found to be favourable for CO_2 adsorption. $[Al_{12}O(OH)_{18}(H_2O)_3(Al_2(OH)_4)(btc)_6]\cdot 24H_2O$ (MIL-96) has shown a moderately high enthalpy of adsorption of 33 kJ/mol,[40] comparable to MIL-53(Al) and MIL-53(Cr) ([M(OH)(bdc)], M = Cr, Al; 35 and 32 kJ/mol, respectively).[41]

B Alkyl Amines

Compounds containing the alkylamine functionality have long been known to enhance specific CO_2 capture from flue gas streams; however, examples in MOFs are relatively limited due to the need for their postsynthetic introduction to preclude issues with the presence of an accessible Lewis basic site during synthesis. A prime example of the issues encountered in the introduction of alkylamine groups during framework synthesis is the incorporation of a chelating nitrogen donor macrocycle into the tricarboxylate ligand used to form the framework $[Zn_2(tcptad)(H_2O)]Cl$.[42] In this case, the Zn^{2+} ions used in the synthesis are bound to both the carboxylate sites (thereby propagating the 3D polymer) and the free nitrogen donors, resulting in the absence of any free alkylamine sites to interact with guest CO_2 molecules. This is evident from the relatively low heat of adsorption (26 kJ/mol at low coverage), indicating weak interactions with the framework surface. Herein, all examples of alkylamine containing MOFs to affect CO_2 adsorption have been achieved post-synthetically. Primarily, such interactions have been characterised by significantly higher adsorption enthalpies in the order of 60-100 kJ/mol. The most common post-synthetic modification (PSM) strategy used to achieve the alkylamine functionality on a solid support involves grafting onto an open metal site, a technique first reported by Ferey, *et al.* for use as a solid base catalyst.[43, 44]

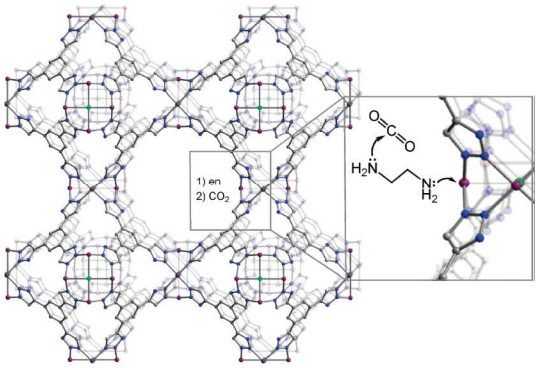

Figure 3. Post-synthetic alkylamine functionalisation as adopted by Long and coworkers. Reprinted with permission from reference 23. Copyright 2009 American Chemical Society.

This approach has been exploited for CO_2 capture purposes by Long and coworkers, first in CuBTTri post-synthetically functionalised with ethylenediamine (en, Figure 3) and *N,N'*-dimethylethylenediamine (mmen) to form en-CuBTTri (Figure 3) and mmen-CuBTTri, respectively.[23, 45] Both materials exhibited reduced surface areas compared to the bare material, but higher CO_2 uptakes at low partial pressures, and greatly improved CO_2/N_2 selectivities. Additionally, unlike the analogous solution state sorbents, such materials are easily regenerated using low energy PSA approaches. A point of interest in comparing the two materials is the improved performance of the secondary amine (mmen) over the primary amine (en) appended material in terms of surface area (870 vs. 345 m^2/g), heat of adsorption of CO_2 (96 vs. 78 kJ/mol), overall CO_2 uptake in the region 0-1 bar and degree of post-synthetic modification (1 mmen/Cu^{2+} site vs. 0.3 en/Cu^{2+} site). While not all of these properties are attributed to amine sterics, it is likely that the higher steric hindrance around the nitrogens in mmen reduces hydrogen bonding between mmen molecules, thereby allowing for a higher degree of PSM and favouring better performance with regard to CO_2 interactions when employing this strategy in microporous systems. Interestingly, introduction of the sterically-hindered secondary amine piperazine appeared to produce frameworks more similar in behaviour to en-CuBTTri than mmen-CuBTTri (i.e., drastic reduction in surface area, lower degrees of PSM and lower heats of adsorption).[46,47]

In a similar way, *N,N'*-dimethylethylenediamine was also employed in an attempt to improve CO_2 uptake in [Mg_2(dobpdc)]. This too resulted in a lower apparent surface area but higher CO_2 capacity at <1 bar as compared to the unappended material.[10] Unusually in this material, a stepped isotherm was observed and was attributed to an unprecedented "amine ordering" effect whereby a hydrogen bonded complex forms across the pore from the two carbamic acid moieties resulting from the sorption of CO_2 onto the secondary amine sites.[48] This material therefore shows a 1:1 amine:CO_2 stoichiometry rather than the 2:1 stoichiometry generally observed in such materials, which is manifested experimentally as a weaker initial binding energy. These interactions have been supported by both experimental and quantum chemical methods.

The introduction of alkylamines to open metal sites in MOFs is particularly useful in designing materials for capture from ultra-dilute and humid CO_2 streams, as more facile regeneration processes may be used compared to those for materials with open metal sites. In functionalising [Mg_2(dobdc)] with varying amounts of ethylenediamine, the low pressure CO_2 uptake, performance in humid conditions and regenerability (Ar purge for 3 h at 110 °C vs high vacuum for 5 h at 250 °C) of the material were improved compared to the bare material.[49]

Using covalent "click chemistry" PSM techniques to generate a triazo-alkyl amine functionality, Zhao and coworkers demonstrated improved ambient pressure CO_2 uptake in the mesoporous material MIL-101 (Figure 4). Interestingly, the heat of adsorption (30 kJ/mol) was significantly lower than that reported in related functionalised materials such as those mentioned above.[50] This may be a result of the large pore size resulting in a lower probability of the CO_2 guest molecules interacting with the binding site. The improved CO_2 uptake of the functionalised material may also arise from a pore size effect (with the functional group effectively lowering the available pore volume/surface area), or an interaction with the nitrogen donors of the triazo link, rather than an interaction with the alkylamine itself. Subtle changes in pore size/volume have been shown to have an effect on CO_2 uptake at ambient pressures and temperatures,[51] although this effect was not explored.

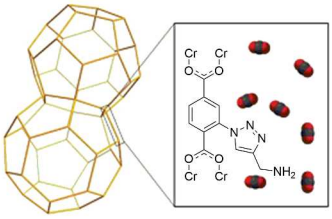

Figure 4. Illustration of ''clicked'' adsorbent, MIL-101-triazo-NH_2, for selective CO_2 capture. Reproduced from Ref. 50 with permission from The Royal Society of Chemistry.

C Aryl Amines, *N*-heterocycles, and other nitrogen-rich MOFs

Aryl amines or nitrogen heterocycles with free nitrogen donors are more readily incorporated into MOFs with predictable topologies, compared with the aforementioned alkylamines. Additionally, many "amino" analogues of unfunctionalised dicarboxylates are commercially available (e.g., 1,4-bdc-NH_2). Hence, "amino tagged" frameworks which are isostructural to their non-functionalised analogues are synthesised directly without the need for PSM, thereby providing a platform by which the effect of functionalisation can be assessed (most notably, the replacement of 1,4-bdc with 1,4-bdc-NH_2 in numerous MOFs such as MIL-101 ([$Cr_3F(H_2O)_2O$(bdc)$_3$]),[52-55] MIL-53 ([M(OH)(bdc)], M = Cr, Al),[56] MIL-68 ([M(OH)(bdc)] M = V, Al, Fe, In),[57] UiO-66 ([$(ZrO)_{24}$(bdc)$_{24}$]),[58, 59] [Zn(bdc)(ted)$_{0.5}$],[60] and USO-2 ([Ni_2(bdc)$_2$(ted)][61]). In all cases, such substitution resulted in higher enthalpies of adsorption for CO_2 and higher uptakes in the low pressure regime (<1 bar), despite a reduction in surface area. As for the case of materials with open metal sites, the higher affinity of amine groups for water compared with their unfunctionalised analogues is often neglected in the discussion of their applications in flue gas capture.[62,63]

MOFs incorporating the naturally occurring ligand adeninate (with a high % of nitrogen donors, so-called "bio-MOFs"), [Zn_8(ad)$_4$(bpdc)$_6$]·0.2X (X = ammonium counterion)[64,65] and [Co_2(ad)$_2$(CO_2CH_3)$_2$][66] (Figure 5) have shown both a favourable affinity for CO_2 at low pressures as well as a high enthalpy of adsorption due to the N-donor density. Additionally, in the anionic framework [Zn_8(ad)$_4$(bpdc)$_6$]0.2X (X = ammonium counterion), the pore size has been modulated by exchanging the ammonium counterion. As in the aforementioned study by Zhang and coworkers,[24] it was shown that smaller pore sizes favoured a high CO_2 enthalpy of adsorption.[65]

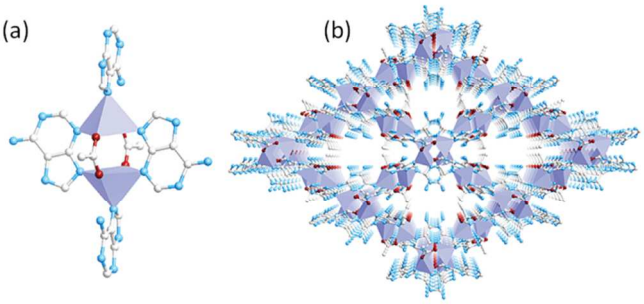

Figure 5. Crystal structure of bio-MOF-11, [Co_2(ad)$_2$(CO_2CH_3)$_2$], showing (a) the Co^{2+}-adeninate-acetate clusters bridged by adeninate to generate (b) an extended 3D porous structure showing channels. Reprinted with permission from reference 66. Copyright 2009 American Chemical Society.

Tetrazole[67-70] and triazole[50,71,72] based ligands have similarly been employed for MOF design due to their "N_2-phobic/CO_2-philic" natures. In all cases, such frameworks with a high density of nitrogen donors (particularly those which are sterically available to donate a lone pair to guest molecules in the pore of the framework creating "open nitrogen donor sites") have been shown to possess high CO_2 uptakes (<1 bar), selectivity over N_2 and moderate enthalpies of adsorption in the order of 25-35 kJ/mol.[70,71,73] Furthermore, in a purely covalent organic polymer, nitrogen rich azo groups were reported to be "N_2-phobic" as well as promoting CO_2 uptake in the low pressure regime ("CO_2-philic").[74]

Aryl amine and N-heterocycle containing MOFs typically exhibit lower enthalpies of adsorption for CO_2 compared with those observed for alkyl amines, and characterisation of a direct interaction between CO_2 and the nitrogen lone pair is

sometimes dubious. For example, Woo and co-workers undertook a simulation in which methyl groups were substituted by the amino group in the ligand aminotriazolate to decouple the electronic effects of the amine group from steric factors. The two groups are isoelectronic and should therefore exhibit similar dispersion interactions, but they have different electron donating abilities. Only a negligible difference in uptake upon substitution was found, consistent with the notion that the amines in this case do not significantly contribute to the CO_2 binding.[75] Notably however, in $[Zn_2(C_2O_4)(C_2N_4H_3)_2]$ incorporating 3-amino-1,2,4-triazole, nitrogen-CO_2 interactions were observed directly by *in situ* single crystal diffraction methods, and have been supported by computational calculations which suggest a cooperative CO_2 binding effect.[76] This highlights the importance of investigating not only electronic but also steric factors.

D Amide/urea moieties

Like the aryl amine functionality, the presence of amide groups is thought to promote CO_2/N_2 selectivity, although the evidence for this is limited to reports of heat of adsorption (no crystallographic or spectroscopic evidence of interaction), which have been found to be in the order of 26–35 kJ/mol. As alluded to previously, pore size plays an important role in addition to the presence of the functional group, whereby smaller pore systems often yield higher enthalpies of adsorption.[77,78] An interesting comparison of two large pore systems of the same topology has been undertaken, one with a ligand containing an amide linker while the other contains a ligand of similar dimensions with an ethylene linker in place of the amide (Figure 6). These two systems exhibit a difference in adsorption enthalpy (26.3 kJ/mol for the amide containing MOF compared to 22 kJ/mol for the ethylene containing MOF at low coverage); furthermore, the amide containing framework showed improved low pressure CO_2 uptake which is attributed to the stronger binding affinity of that linker. This study provides good evidence of an interaction between CO_2 and the amide group from heat of adsorption data alone, despite no direct *in situ* spectroscopic or diffraction studies.[77]

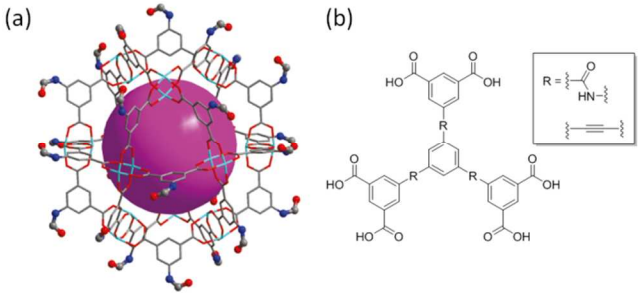

Figure 6. (a) Portion of the structure of the (3,24)-connected rht-type framework showing surface decoration by acylamide groups. (b) Comparison of two ligands incorporated into this framework topology incorporating the amide vs. the ethylene bridge. Reprinted with permission from reference 77. Copyright 2010 American Chemical Society.

E Carboxylic acids

MOFs incorporating uncoordinated carboxylic acids, as one of the most polar functional groups studied, have displayed excellent improvements in CO_2/N_2 selectivity, CO_2 heat of adsorption ($|Q_{st}|$ in the order 33 – 36 kJ/mol) and low pressure CO_2 uptake in numerous systems compared to their non-functionalised analogues, or analogues functionalised with different (lower polarity) functional groups.[59, 79-81] Despite this, no specific structural data have been cited for the interaction between uncoordinated carboxylic acid groups and guest CO_2 molecules.

F Sulfonic acids

Like carboxylic acid-functionalised materials, sulfonic acid-functionalised MOFs display higher heats of adsorption than their unfunctionalised analogues (in the order of 30-34 kJ/mol), good low pressure CO_2 uptake and CO_2/N_2 selectivities due to the polar nature of the functional group.[59] Interestingly, exchanging the acidic proton for Li^+ has been shown to increase the heat of adsorption from ~30 to ~35 kJ/mol in a porous polymer network.[82] Sulfonic acid groups have also been shown to decrease H_2O uptake with respect to other polar functional groups when incorporated into materials with the same topology.[62]

G Hydroxyl groups

Hydroxyl functionalised MOFs, when compared to their unfunctionalised analogues, show a small improvement in heat of adsorption (~3-5 kJ/mol higher than analogues with a hydrogen atom in its place; reported values between 23.2-29.4 kJ/mol) and in low pressure CO_2 uptake.[50,59,60,80] Additionally, such analogues have been shown to outperform their aryl amine counterparts in terms of heat of adsorption.[59,60,80] Due to the marginal improvement in performance, and lack of other evidence suggesting a direct electronic interaction between the polar group and the CO_2 guests, it is not clear whether a direct interaction is responsible for this improvement, or if it is due to other (e.g., steric) factors. Ionic hydroxide groups act as stronger sorption sites; for example, in MIL-53, DFT calculations have shown that CO_2 molecules interact directly with the hydroxide groups bound to the Cr^{3+} metal clusters, whereby the O(CO_2)–H(OH) distance was 2.19 Å and a linear O=C=O···H fragment was observed.[83] In this case, a higher heat of adsorption (32 kJ/mol) was also observed.[41]

H Nitro groups

Nitro groups have been shown to improve CO_2 uptake and $|Q_{st}|$ in the low pressure regime with respect to their unfunctionalised analogues in ZIF structures,[84] MIL-101[55] and UiO-66.[58,59] In general, nitro groups do not improve low pressure CO_2 uptake as much as an NH_2 group in their place, but they do improve $|Q_{st}|$ more than their aryl amine analogues due to their increased polarity. Additionally, NO_2 functionalised MIL-101 has been found to have a lower affinity for water than its unfunctionalised analogue,[62] which may be advantageous for the implementation of such functionalised materials in flue gas capture.

I Halogen groups

There is limited evidence to demonstrate that aryl halogen groups themselves provide any enhancement to low pressure

CO_2 uptake and heat of adsorption (increases reported with respect to non-functionalised analogues are in the order of ~2 kJ/mol).[59,85] This small increase is likely to arise as an effect of the increased steric bulk in the pore, rather than any interaction between CO_2 molecules and the functional group.

Incorporation of CF_3 into ligands has been a popular approach to introducing halogens into MOFs for gas sorption;[86-90] however, the evidence of a direct interaction with the CF_3 group is dubious (low heats of interaction with $|Q_{st}|$ = 22.2 – 22.9 kJ/mol in the absence of other binding sites) and the pore constriction resulting from this group is a more likely explanation for small enhancements in low pressure uptake and heats of adsorption than any direct interaction with CF_3 itself. These groups are thought to improve the hydrophobicity/water stability of the MOFs into which they are incorporated;[89] however, water sorption data only indicate a modest enhancement in hydrophobicity in such materials, owing to the different behaviour of water vapour compared with liquid water.[90]

J Ionic MOFs

The charged framework surfaces present in ionic frameworks are thought to enhance CO_2-framework interactions; however, it is sometimes difficult to decouple these surface effects from the presence of metal sites and counterions in the pore space. As such, reported heats of adsorption are highly variable, and trends are difficult to discern. $[Ni_2(bpy)_3(NO_3)_4]$ has been found to have excellent low pressure CO_2 uptake, with steps in the isotherm at low surface coverage associated with a slowing in the adsorption kinetics.[91] In anionic frameworks incorporating both NH_4^+ counterions and nitrogen heterocycles with uncoordinated N donor sites which point into a small pore, heats of adsorption have been reported to be as high as 35 kJ/mol.[65,71] In a similarly charged framework containing open metal binding sites rather than N donor sites, and a similar ammonium counterion in the pore, heats of adsorption reached a maximum of 25-27 kJ/mol. This suggests that the charged nature of the framework plays a secondary role in influencing CO_2 binding compared to other (stronger) binding sites in the material and the influence of pore size.[24] These values are lower than those typically observed in zeolites where the predominant interaction is with the charged surface ($|Q_{st}|$ = 30 – 50 kJ/mol).[92]

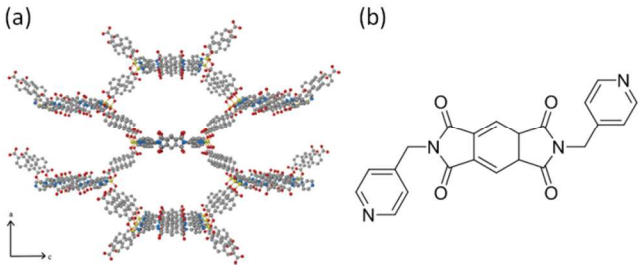

Figure 7. (a) [Zn(ndc)(dpmbi)] and (b) the redox-active dpmbi ligand, the reduction of which results in an anionic framework. Reproduced from Ref. 93 with permission from The Royal Society of Chemistry.

Another approach to generating ionic frameworks is through the incorporation of a redox-active ligand. Upon reducing the framework, a positive ion (typically an alkali earth metal) is introduced into the pore which may act to enhance sorbent-sorbate interactions.[94-96] Increased stoichiometric reduction (i.e., a higher ratio of counterions in the framework pore) has been found to displace interpenetrated frameworks, thereby increasing not only the CO_2 selectivity and heat of adsorption, but also significantly increasing absolute uptake.[97] In the framework [Zn(ndc)(dbmbi)] (Figure 7), varying amounts of the reductant sodium napthalanide was used to identify the "optimal" balance between the displacement of the interpenetrated framework and optimal sorbent-sorbate interactions. A maximum $|Q_{st}|$ of 29 kJ/mol (compared to 23 kJ/mol for the neutral framework) was identified, and the selectivities of all of the reduced species were improved compared to their neutral counterpart. This study highlighted the versatility and tunability of this type of redox-active system, and suggested its potential application in redox-based swing processes.[93]

K Hydrophobic groups

Given the impact of pore size and the often non-specific nature of CO_2-framework interactions in the presence of polar functional groups, it may be possible to mediate the heat of adsorption simply by introducing a bulky group to the pore (as in the case of CF_3, *vide supra*). Furthermore, if this group is hydrophobic in nature, it may give rise to increased water resistance, as discussed above with respect to open metal sites. The introduction of alkyl[80, 98, 99] or alkoxy[58, 100] groups have been shown to improve CO_2/N_2 selectivity, and have a small impact on increasing the heat of adsorption in MOFs by ~2-5 kJ/mol over an unfunctionalised analogue. The presence of such hydrophobic functionalities have also been shown to improve the stability of frameworks with low hydrothermal stability in their native state;[101,102] as well, they have been found to exhibit lower water sorption at various relative humidities (a significant problem often neglected in the research of MOFs for CO_2 capture from flue gas streams)[98,99] to the point of producing "super hydrophobic" MOFs.[103]

Conclusions

In summary, the aforementioned examples of materials incorporating functional sites highlight the need to consider steric as well as electronic effects of the functional group. This is particularly critical for microporous systems, where the presence of a functional group can significantly alter the sterics of the pore space. The accessibility of a functional site must also be considered, and this has been shown to be particularly problematic for interpenetrated systems.[104] The systematic comparison of various functional sites in a given MOF topology are rare but informative, and the limited studies conducted to-date in this regard indicate a relationship between the polarity of the group and the heat of adsorption (see for example Figure 8 which shows the variation of $|Q_{st}|$ (denoted ΔH_{ads} in this case) for the functionalised analogues of MIL-53).[58,80] The importance of measurements of the water affinity of such materials is garnering attention, with mixed stream and breakthrough experiments under humid conditions becoming increasingly common.[31]

Clearly, the development of ideal candidate MOFs for postcombustion flue gas capture relies on a number of factors between which a trade-off exists. The magnitude of $|Q_{st}|$ provides key insights into the performance of a material as it reflects the low pressure (<1 bar) uptake, as well as the CO_2 selectivity over other gases (e.g., N_2, CH_4). The comparisons

drawn in this highlight article have sought to provide a roadmap for the future development of functionalised MOFs in which these key parameters can be refined and optimised.

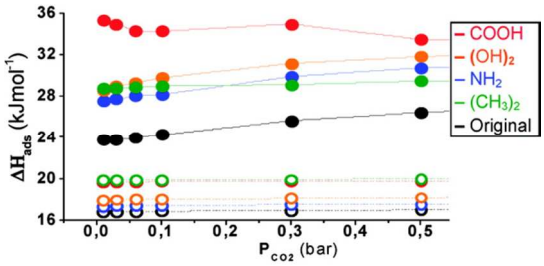

Figure 8. Comparison of heats of adsorption for differently functionalised analogues of MIL-53. Reprinted with permission from reference 80. Copyright 2010 American Chemical Society.

Table 1. Table of CO_2 heat of adsorption and coordination environments in MOFs containing various functional sites. Where applicable, the heat of adsorption of the unfunctionalised analogue is provided in parentheses for comparison. * denotes values derived from GCMC calculations.

	MOF	Pore volume (cm^3/g)	Binding site	Coordination environment	$\lvert Q_{st} \rvert$ (kJ/mol)	Ref
A	$[Cu_3(btc)_2]$ (HKUST-1)	0.79	Cu^{2+}	5-coordinate "Cu paddlewheel" motif (4 coordinate on desolvation), O donors	30	13
A	$[Mg_2(dobdc)]$	0.65	Mg^{2+}	Octahedral (square pyramidal on desolvation), O donors	47	25
					39	27
					42	34
A	$[Ni_2(dobdc)]$	0.48	Ni^{2+}	Octahedral (square pyramidal on desolvation), O donors	41	25
					38	34
A	$[Co_2(dobdc)]$		Co^{2+}	Octahedral (square pyramidal on desolvation), O donors	37	25
					34	34
A	$[Zn_2(dobdc)]$		Zn^{2+}	Octahedral (square pyramidal on desolvation), O donors	30	34
A	$[Mn_2(dobdc)]$		Mn^{2+}	Octahedral (square pyramidal on desolvation), O donors	31	34
A	$[Fe_2(dobdc)]$		Fe^{2+}	Octahedral (square pyramidal on desolvation), O donors	34	34
A	$[Cu_2(dobdc)]$		Cu^{2+}	Octahedral (square pyramidal on desolvation), O donors	24	34
A	$H_3[(Cu_4Cl)_3(BTTri)_8]$ (CuBTTri)		Cu^{2+}	Octahedral (square pyramidal on desolvation), equatorial N donors, axial choride ion	21	23
A	$[Cd_2(pfpdia)]$	0.11	Cd^{2+}	Octahedral, O-donors	36	87
A	$[Cu_2(tcm)]$ (SNU-21)	0.31	Cu^{2+}	5-coordinate "Cu paddlewheel" motif (4 coordinate on desolvation), O donors	36	22
A	[Cr(btc)] (MIL-100)	1.1	Cr^{3+}	Octahedral, O-donors	63	39
A	$[Cr_2(bdc)_3]$ (MIL-101)	2.15	Cr^{3+}	Octahedral, O-donors	44	39
A	$[Al_{12}O(OH)_{18}(H_2O)_3(Al_2(OH)_4)(btc)_6]$ (MIL-96(Al))		Al^{3+}	Octahedral, O-donors	33	40
A	$[Mg_2(dobpdc)]$	1.25	Mg^{2+}	Octahedral (square pyramidal on desolvation), O donors	44	10
A	$[Cu_4(mttbpdc)]$ (NOTT-140)	1.05	Cu^{2+}	5-coordinate "Cu paddlewheel" motif (4 coordinate on desolvation), O donors	24	21

A	$Co[Co(CN)_6]_2$		Co^{2+}	Octahedral, N-donors	28	37
A	$Zn[Co(CN)_6]_2$		Zn^{2+}	Octahedral, N-donors	29	37
A	$Ni[Co(CN)_6]_2$		Ni^{2+}	Octahedral, N-donors	54	36
A	$Cu[Co(CN)_6]_2$		Cu^{2+}	Octahedral, N-donors	49	36
A	$Mn[Co(CN)_6]_2$		Mn^{2+}	Octahedral, N-donors	67	36
A	$X_3[(Cu_4Cl)_3(btc)_8]$ where		Cu^{2+}	Octahedral, O-donors and an axial chloride		24
	X = dimethylammonium	0.341			25	
	= tetramethylammonium,				27	
	= tetrapropylammonium				25	
A	$[Zn_4(OH)_2(1,2,4\text{-btc})_2]$	0.205	Zn^{2+}	Tetrahedral zinc centre with 4 O-donors	20.2	105
B	$H_3[(Cu_4Cl)_3(BTTri)_8(en)_5]$(en-CuBTTri		Alkyl-NH_2		78	23
B	$H_3[(Cu_4Cl)_3(BTTri)_8(mmen)_{12}]$(mmen-CuBTTri)	0.363	Alkyl-NHMe		96	45
B	$[Mg_2(dobpdc)(mmen)_{1.6}(H_2O)_{0.4}]$		Alkyl-NHMe		71	10
B	$H_3[(Cu_4Cl)_3(BTTri)_8(pip)_{12}]$ (pip-CuBTTri)		Alkyl-NHMe		96	46
B	$[Ni_2(dobdc)(pip)_{0.5}]$		Alkyl-NHMe		46	47
B	$[Cr_3F(H_2O)_2O(bdc\text{-}triazoNH_2)_3]$ (MIL-101-triazoNH_2(Cr))		Alkyl-NH_2		30	50
C	$[Cr_3F(H_2O)_2O(bdc\text{-}NH_2)_3]$ (MIL-101-NH_2(Cr))	2.26	Aryl-NH_2		43 (44)	52-55
C	$[In(OH)(bdc\text{-}NH_2)]$		Aryl-NH_2		24 (15)	57
C	$[ZrO(bdc\text{-}NH_2)]$ (UiO-66-NH_2)	0.40 (0.45)	Aryl-NH_2		29 (26)*	58, 59
C	$[Zn(bdc\text{-}NH_2)(ted)_{0.5}]$	0.46 (0.75)	Aryl-NH_2		23 (20)	60
C	$[Al(OH)(bdc\text{-}NH_2)]$ (USO-1-NH_2, MIL-53-NH_2)	0.25 (0.42)	Aryl-NH_2		50 (30)	61
C	$[Zn_8(ad)_4(bpdc)_6]$0.2X (bio-MOF-1)		Nitrogen heterocycle with free N-donors			64, 65
	X = dimethylammonium	0.75			22	
	= tetramethylammonium	0.65			24	
	= tetraethylammonium	0.55			27	

	= tetrabutylammonium	0.37		32	
C	$[Co_2(ad)_2(CO_2CH_3)_2]$	0.45	Nitrogen heterocycle with free N-donors	45	66
C	$[Co(dpt24)_2]$ (MAF-25)	0.86	Nitrogen heterocycle with free N-donors	26	73
C	$[Co(mdpt24)_2]$ (MAF-26)	0.81	Nitrogen heterocycle with free N-donors	23	73
C	$(Me_2NH_2)[Co_3Cl_4(ppt)_2]$		Nitrogen heterocycle with free N-donors	33-35	71
C	$[Zn(CN_5H_2)_2]$ (ZTF-1)		Nitrogen heterocycle with free N-donors	25	70
D	$[Cu_{24}(tpbtm)]$	1.27	Amide linker	26 (22)	77
D	[Cu(inaip)]		Amide linker	35	78
E	[ZrO(bdc-COOH)] (UiO-66-COOH)	0.31 (0.45)	Aryl-COOH	33 (26)*	59
E	$[ZrO(bdc\text{-}(COOH)_2)]$ (UiO-66-$(COOH)_2$)	0.26 (0.45)	Aryl-COOH	35 (26)	81
E	[Al(OH)(bdc-COOH)] (MIL-53-COOH)		Aryl-COOH	35 (23)*	80
F	$[ZrO(bdc\text{-}SO_3H)]$ (UiO-66-SO_3H)	0.25	Aryl-SO_3H	34 (26)	59
F	PPN-6-SO_3H	0.58 (2.44)	Aryl-SO_3H	30 (17)	82
F	PPN-6-SO_3Li	0.52 (2.44)	Aryl-SO_3H	36 (17)	82
G	$[Zn(bdc\text{-}OH)(TED)_{0.5}]$	0.56 (0.75)	Aryl-OH	23 (20)	60
G	$[ZrO(bdc\text{-}(OH)_2)]$ (UiO-66-$(OH)_2$	0.36	Aryl-OH	29 (26)*	59
G	$[Al(OH)(bdc\text{-}(OH)_2)]$ (MIL-53-$(OH)_2$)		Aryl-OH	29 (23)*	80
G	[Cr(OH)(bdc)] (MIL-53)		Metal-hydroxide	32	41
H	$[ZrO(bdc\text{-}NO_2)]$ (UiO-66-NO_2) (theoretical)	0.32	Aryl-NO_2	31 (26)*	59
H	$[ZrO(bdc\text{-}NO_2)]$ (UiO-66-NO_2) (experimental)	0.32	Aryl-NO_2	32 (26)	58
I	[ZrO(bdc-Br)] (UiO-66-Br)	0.30 (0.45)	Aryl-Br	28 (26)*	59
I	$[ZrO(bdc\text{-}(CF_3)_2)]$ (UiO-66-$(CF_3)_2$)	0.22 (0.45)	Aryl-CF_3	34 (26)*	59

I	$[Zr_6(Cl_2AzoBDC)]$	0.94 (0.51)	Aryl-Cl	22 (20)*	85
I	$[Cd_2(pfpdia)]$	0.11	Alkyl-CF_3, Cd^{2+}	37 (attributed to Cd^{2+} sites)	87
I	$[Zn_{2.66}O_{0.66}(bpdc\text{-}(CF_3)_2)_2]$	0.310	Aryl-CF_3	23	89
I	$[Cu_2(ftpta)]$	0.810	Aryl-CF_3	22 (24)	88
J	$(Me_2NH_2)(Hdmf)[Co_3Cl_4(pt)_2]$		Anionic framework	33–35	71
J	$[Zn_8(ad)_4(bpdc)_6]0.2X$ (bio-MOF-1)		Anionic framework		64, 65
	X = dimethylammonium	0.75		22	
	= tetramethylammonium	0.65		24	
	= tetraethylammonium	0.55		27	
	= tetrabutylammonium	0.37		31	
J	$X_3[(Cu_4Cl)_3(btc)_8]$ where		Anionic framework		24
	X = dimethylammonium	0.341		25	
	= tetramethylammonium	0.282		27	
	= tetrapropylammonium	0.142		26	
J	[Zn(ndc)(dpmbi)]·XNa		Anionic framework		93
	X = 0			23	
	= 0.109			26	
	= 0.233			29	
	= 0.367			15	
	= 0.378			29	
K	$[Al(OH)(bdc\text{-}(CH_3)_2)]$ (MIL-53-$(CH_3)_2$(Al))		Aryl-CH_3	29 (23)*	80
K	$[ZrO(bdc\text{-}(CH_3)_2)]$ (UiO-66-$(CH_3)_2$)		Aryl-CH_3	47 (26)	98
K	$[ZrO(bdc\text{-}(OMe)_2)]$ (UiO-66-$(OMe)_2$)	0.38	Aryl-OCH_3	32 (26)	58

List of abbreviations H_8mttbpdc = 4',4''',4''''',4''''''-methanetetrayltetrakis(([1,1'-biphenyl]-3,5-dicarboxylate)), H_4tcm = tetrakis[4-(carboxyphenyl)-oxamethyl] acid, H_3BTTri = 1,3,5-tris(1*H*-1,2,3-triazol-5-yl)benzene, H_3btc = benzene-1,3,5-tricarboxylic acid, H_4dobdc = 2,4-dihydroxyterephthalic acid, H_4dobpdc = 4,4′-dihydroxy-3,3′-biphenyldicarboxylic acid, tcptad = 1,4,7-tris(4-carboxyphenyl)-1,4,7-triazonane-1,4-diium, en = ethylenediamine, mmen = *N,N'*-dimethylethylenediamine, pip = piperazine, H_2bdc = 1,4-biphenyldicarboxylic acid, H_2bdc-NH_2 = 2-aminoterephthalic acid, ted = 1,4-diazabicyclo[2.2.2]octane, ad = adeninate, H_2bpdc = 4,4'-biphenyldicarboxylic acid, bpy = 4,4'-bipyridine, H_2ndc = naphthalene-2,6-dicarboxylic acid, dpmbi = N,N'-di-(4-pyridylmethyl)-1,2,4,5-benzenetetracarboxydiimide, H_4pfpdia = 4,4'-(perfluoropropane-2,2-diyl)diphthalic acid, 1,2,4-btc = benzene-1,2,4-tricarboxylate, dpt24 = 3-(2-pyridyl)-5-(4-pyridyl)-1,2,4-triazolate, mdpt24 =

3-(3-methyl-2-pyridyl)-5-(4-pyridyl)-1,2,4-triazolate, H_2ppt = 3-(2-phenol)-5-(4-pyridyl)-1,2,4-triazole, tpbtm = N,N′,N′′-tris(isophthalyl)-1,3,5-benzenetricarboxamide, H_2inaip = 5-(isonicotinamido) isophthalic acid, bpdc-$(CF_3)_2$ = 2,2′-bis-trifluoromethyl-biphenyl-4,4′-dicarboxylate, ftpta = 5'-(trifluoromethyl)-[1,1':3',1"-terphenyl]-3,3",5,5"-tetracarboxylic acid, H_2bdc-COOH = 1,2,4-benzenetricarboxylic acid, H_2bdc-$(COOH)_2$ = 1,2,4,5-benzenetetracarboxylic acid, H_2bdc-SO_3H = 2-sulfoterephthalic acid, H_2bdc-NO_2 = 2-nitroterephthalic acid, H_2bdc-$(CF_3)_2$ = 2,5-bis(trifluoromethyl)terephthalic acid, H_2bdc-Br = 2-bromoterephthalic acid, Cl_2AzoBDC = *(E)*-4,4'-(diazene-1,2-diyl)bis(2-chlorobenzoic acid), H_2bdc-triazoNH_2 = 2-(4-(aminomethyl)-1*H*-1,2,3-triazol-1-yl)terephthalic acid

LIGANDS THAT GENERATE MATERIALS WITH OPEN METAL SITES

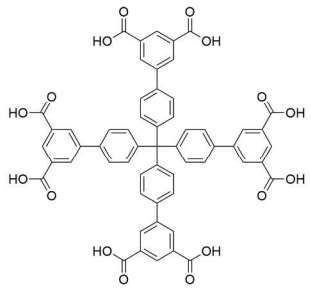

H_8mttbpdc = 4',4''',4''''',4'''''''-methanetetrayltetrakis(([1,1'-biphenyl]-3,5-dicarboxylic acid))

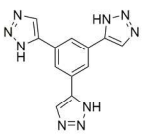

H_3BTTri = 1,3,5-tris(1*H*-1,2,3-triazol-5-yl)benzene

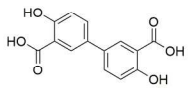

H_4dobpdc = 4,4'-dihydroxy-3,3'-biphenyldicarboxylic acid

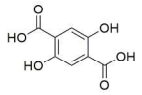

H_4dobdc = 2,5-dihydroxyterephthalic acid

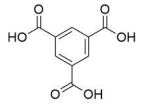

H_3btc = benzene-1,3,5-tricarboxylic acid

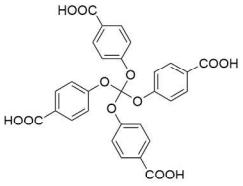

H_4tcm = 4,4',4'',4'''-(methanetetrayltetrakis(oxy))tetrabenzoic acid

REDOX ACTIVE

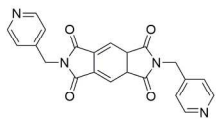

dpmbi = N,N'-di-(4-pyridylmethyl)-1,2,4,5-benzenetetracarboxdiimide

AMIDE/UREA

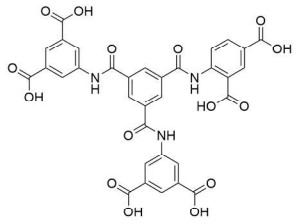

H_6tpbtm = N,N',N''-tris(isophthalyl)-1,3,5-benzenetricarboxamide

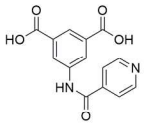

H_2inaip = 5-(isonicotinamido) isophthalic acid

COMMON LIGANDS/UNFUNCTIONALISED CO-LIGANDS

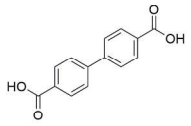

H_2bpdc = 4,4'-biphenyldicarboxylic acid

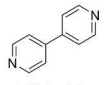

4,4'-bipyridine

ted = 1,4-diazabicyclo[2.2.2]octane

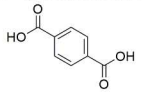

H_2bdc = 1,4-benzenedicarboxylic acid

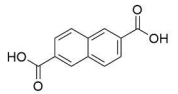

H_2bdc = naphthalene-2,6-dicarboxylic acid

ALKYL AMINES

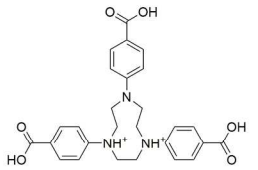

H_5tcptad = 1,4,7-tris(4-carboxyphenyl)-1,4,7-triazonane-1,4-diium

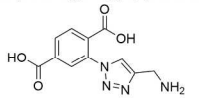

H_2bdc-triazoNH$_2$ = 2-(4-(aminomethyl)-1H-1,2,3-triazol-1-yl)terephthalic acid

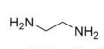

en = ethylenediamine

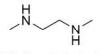

mmen = *N,N'*-dimethylethylenediamine

EXAMPLES OF BDC DERIVATIVES

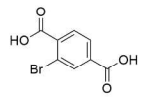

H_2bdc-Br = 2-bromoterephthalic acid

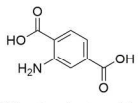

H_2bdc-NH$_2$ = 2-aminoterephthalic acid

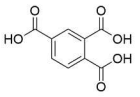

H_2bdc-(COOH) = benzene-1,2,4-tricarboxylic acid

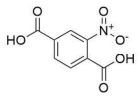

H_2bdc-NO$_2$ = 2-nitroterephthalic acid

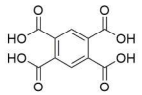

H_2bdc-(COOH)$_2$ = 1,2,4,5-benzenetetracarboxylic acid

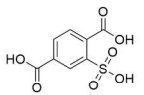

H_2bdc-SO$_3$H = 2-sulfoterephthalic acid

HALOGEN GROUPS

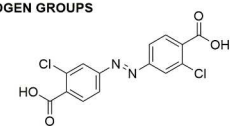

Cl_2AzoBDC = (*E*)-4,4'-(diazene-1,2-diyl)bis(2-chlorobenzoic acid)

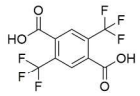

H_2bdc-(CF$_3$)$_2$ = 2,5-bis(trifluoromethyl)terephthalic acid

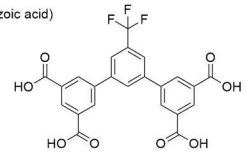

H_4ftpta = 5'-(trifluoromethyl)-[1,1':3',1''-terphenyl]-3,3'',5,5''-tetracarboxylic acid

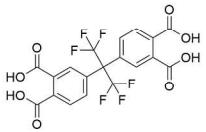

H_4pfpdia = 4,4'-(perfluoropropane-2,2-diyl)diphthalic acid

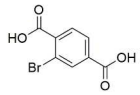

H_2bdc-Br = 2-bromoterephthalic acid

H_2bpdc-(CF$_3$)$_2$ = 2,2'-bis-trifluoromethyl-biphenyl-4,4'-dicarboxylic acid

ARYL AMINES, N-HETEROCYCLES AND N-RICH

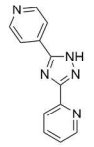

Hdpt24 = 3-(2-pyridyl)-5-(4-pyridyl)-1,2,4-triazole

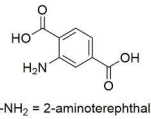

H_2bdc-NH$_2$ = 2-aminoterephthalic acid

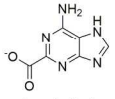

ad = adeninate

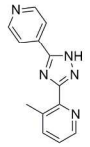

Hmdpt24 = 3-(3-methyl-2-pyridyl)-5-(4-pyridyl)-1,2,4-triazole

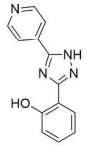

H_2ppt = 3-(2-phenol)-5-(4-pyridyl)-1,2,4-triazole

Acknowledgements

We gratefully acknowledge support from the Science and Industry Endowment Fund.

Notes and references

[a] School of Chemistry F11
University of Sydney NSW 2006 Australia

† Footnotes should appear here. These might include comments relevant to but not central to the matter under discussion, limited experimental and spectral data, and crystallographic data.

1. D. M. D'Alessandro, B. Smit and J. R. Long, *Angew. Chem., Int. Ed.*, 2010, **49**, 6058-6082.
2. J.-R. Li, R. J. Kuppler and H.-C. Zhou, *Chem. Soc. Rev.*, 2009, **38**, 1477-1504.
3. J.-R. Li, Y. Ma, M. C. McCarthy, J. Sculley, J. Yu, H.-K. Jeong, P. B. Balbuena and H.-C. Zhou, *Coord. Chem. Rev.*, 2011, **255**, 1791-1823.
4. J. Liu, P. K. Thallapally, B. P. McGrail, D. R. Brown and J. Liu, *Chem. Soc. Rev.*, 2012, **41**, 2308-2322.
5. K. Sumida, D. L. Rogow, J. A. Mason, T. M. McDonald, E. D. Bloch, Z. R. Herm, T.-H. Bae and J. R. Long, *Chem. Rev.*, 2011, **112**, 724-781.
6. Z. Zhang, Y. Zhao, Q. Gong, Z. Li and J. Li, *Chem. Commun.*, 2013, **49**, 653-661, all references therein.
7. R. Mohr and M. B. Rao, *J. Phys. Chem. B*, 1999, **103**, 6539-6546.
8. Y.-S. Bae and R. Q. Snurr, *Angew. Chem., Int. Ed.*, 2011, **50**, 11586-11596.
9. D. W. Hand, S. Loper, M. Ari and J. C. Crittenden, *Environ. Sci. Technol.*, 1985, **19**, 1037-1043.
10. T. M. McDonald, W. R. Lee, J. A. Mason, B. M. Wiers, C. S. Hong and J. R. Long, *J. Am. Chem. Soc.*, 2012, **134**, 7056-7065.
11. A. Das, D. M. D'Alessandro and V. K. Peterson, in *Energy and Materials* eds. G. Kearly and V. K. Peterson, Springer, 2014, in press
12. S. S.-Y. Chui, S. M.-F. Lo, J. P. H. Charmant, A. G. Orpen and I. D. Williams, *Science*, 1999, **283**, 1148-1150.
13. Z. Liang, M. Marshall and A. L. Chaffee, *Energy Fuels*, 2009, **23**, 2785-2789.
14. S. Bordiga, L. Regli, F. Bonino, E. Groppo, C. Lamberti, B. Xiao, P. S. Wheatley, R. E. Morris and A. Zecchina, *Phys. Chem. Chem. Phys.*, 2007, **9**, 2676-2685.
15. A. Ö. Yazaydın, A. I. Benin, S. A. Faheem, P. Jakubczak, J. J. Low, R. R. Willis and R. Q. Snurr, *Chem. Mater.*, 2009, **21**, 1425-1430.
16. D. Yuan, D. Zhao, D. Sun and H.-C. Zhou, *Angew. Chem., Int. Ed.*, 2010, **49**, 5357-5361.
17. B. Mu, F. Li and K. S. Walton, *Chem. Commun.*, 2009, 2493-2495.
18. X. Liu, M. Park, S. Hong, M. Oh, J. W. Yoon, J.-S. Chang and M. S. Lah, *Inorg. Chem.*, 2009, **48**, 11507-11509.
19. O. K. Farha, A. Özgür Yazaydın, I. Eryazici, C. D. Malliakas, B. G. Hauser, M. G. Kanatzidis, S. T. Nguyen, R. Q. Snurr and J. T. Hupp, *Nat. Chem.*, 2010, **2**, 944-948.
20. Z. Guo, H. Wu, G. Srinivas, Y. Zhou, S. Xiang, Z. Chen, Y. Yang, W. Zhou, M. O'Keeffe and B. Chen, *Angew. Chem., Int. Ed.*, 2011, **50**, 3178-3181.
21. C. Tan, S. Yang, N. R. Champness, X. Lin, A. J. Blake, W. Lewis and M. Schroder, *Chem. Commun.*, 2011, **47**, 4487-4489.
22. T. K. Kim and M. P. Suh, *Chem. Commun.*, 2011, **47**, 4258-4260.
23. A. Demessence, D. M. D'Alessandro, M. L. Foo and J. R. Long, *J. Am. Chem. Soc.*, 2009, **131**, 8784-8786.
24. Y.-X. Tan, Y.-P. He and J. Zhang, *Chem. Commun.*, 2011, **47**, 10647-10649.
25. S. R. Caskey, A. G. Wong-Foy and A. J. Matzger, *J. Am. Chem. Soc.*, 2008, **130**, 10870-10871.
26. X. Kong, E. Scott, W. Ding, J. A. Mason, J. R. Long and J. A. Reimer, *J. Am. Chem. Soc.*, 2012, **134**, 14341-14344.
27. D. Britt, H. Furukawa, B. Wang, T. G. Glover and O. M. Yaghi, *Proc. Nat. Acad. Sci*, 2009, **106**, 20637-20640.
28. Z. R. Herm, J. A. Swisher, B. Smit, R. Krishna and J. R. Long, *J. Am. Chem. Soc.*, 2011, **133**, 5664-5667.
29. J. A. Mason, K. Sumida, Z. R. Herm, R. Krishna and J. R. Long, *En. Environ. Sci.*, 2011, **4**, 3030-3040.
30. P. D. C. Dietzel, V. Besikiotis and R. Blom, *J. Mater. Chem.*, 2009, **19**, 7362-7370.
31. A. C. Kizzie, A. G. Wong-Foy and A. J. Matzger, *Langmuir*, 2011, **27**, 6368-6373.
32. P. D. C. Dietzel, R. E. Johnsen, H. Fjellvag, S. Bordiga, E. Groppo, S. Chavan and R. Blom, *Chem. Commun.*, 2008, 5125-5127.
33. R. Sanz, F. Martinez, G. Orcajo, L. Wojtas and D. Briones, *Dalton Trans.*, 2013, **42**, 2392-2398.
34. D. Yu, A. O. Yazaydin, J. R. Lane, P. D. C. Dietzel and R. Q. Snurr, *Chem. Sci.*, 2013, **4**, 3544-3556.
35. W. Zhou, H. Wu and T. Yildirim, *J. Am. Chem. Soc.*, 2008, **130**, 15268-15269.
36. R. K. Motkuri, P. K. Thallapally, B. P. McGrail and S. B. Ghorishi, *CrystEngComm*, 2010, **12**, 4003-4006.
37. P. K. Thallapally, R. K. Motkuri, C. A. Fernandez, B. P. McGrail and G. S. Behrooz, *Inorg. Chem.*, 2010, **49**, 4909-4915.
38. S. H. Ogilvie, S. G. Duyker, P. D. Southon, V. K. Peterson and C. J. Kepert, *Chem. Commun.*, 2013, **49**, 9404-9406.
39. P. L. Llewellyn, S. Bourrelly, C. Serre, A. Vimont, M. Daturi, L. Hamon, G. De Weireld, J.-S. Chang, D.-Y. Hong, Y. Kyu Hwang, S. Hwa Jhung and G. Férey, *Langmuir*, 2008, **24**, 7245-7250.
40. T. Loiseau, L. Lecroq, C. Volkringer, J. Marrot, G. Férey, M. Haouas, F. Taulelle, S. Bourrelly, P. L. Llewellyn and M. Latroche, *J. Am. Chem. Soc.*, 2006, **128**, 10223-10230.
41. S. Bourrelly, P. L. Llewellyn, C. Serre, F. Millange, T. Loiseau and G. Férey, *J. Am. Chem. Soc.*, 2005, **127**, 13519-13521.
42. G. Ortiz, S. Brandès, Y. Rousselin and R. Guilard, *Chem. Eur. J*, 2011, **17**, 6689-6695.
43. Y. K. Hwang, D.-Y. Hong, J.-S. Chang, S. H. Jhung, Y.-K. Seo, J. Kim, A. Vimont, M. Daturi, C. Serre and G. Férey, *Angew. Chem., Int. Ed.*, 2008, **47**, 4144-4148.
44. D.-Y. Hong, Y. K. Hwang, C. Serre, G. Férey and J.-S. Chang, *Adv. Funct. Mater.*, 2009, **19**, 1537-1552.
45. T. M. McDonald, D. M. D'Alessandro, R. Krishna and J. R. Long, *Chem. Sci.*, 2011, **2**, 2022-2028.

46. A. Das, M. Choucair, P. D. Southon, J. A. Mason, M. Zhao, C. J. Kepert, A. T. Harris and D. M. D'Alessandro, *Microporous Mesoporous Mater.*, 2013, **174**, 74-80.
47. A. Das, P. D. Southon, M. Zhao, C. J. Kepert, A. T. Harris and D. M. D'Alessandro, *Dalton Trans.*, 2012, **41**, 11739-11744.
48. N. Planas, A. L. Dzubak, R. Poloni, L.-C. Lin, A. McManus, T. M. McDonald, J. B. Neaton, J. R. Long, B. Smit and L. Gagliardi, *J. Am. Chem. Soc.*, 2013, **135**, 7402-7405.
49. S. Choi, T. Watanabe, T.-H. Bae, D. S. Sholl and C. W. Jones, *J. Phys. Chem. Lett.*, 2012, **3**, 1136-1141.
50. P.-Z. Li, X.-J. Wang, R. H. D. Tan, Q. Zhang, R. Zou and Y. Zhao, *RSC Adv.*, 2013, **3**, 15566-15570.
51. C. Hon Lau, R. Babarao and M. R. Hill, *Chem. Commun.*, 2013, **49**, 3634-3636.
52. D. Jiang, L. L. Keenan, A. D. Burrows and K. J. Edler, *Chem. Commun.*, 2012, **48**, 12053-12055.
53. T. Devic, P. Horcajada, C. Serre, F. Salles, G. Maurin, B. Moulin, D. Heurtaux, G. Clet, A. Vimont, J.-M. Grenèche, B. L. Ouay, F. Moreau, E. Magnier, Y. Filinchuk, J. Marrot, J.-C. Lavalley, M. Daturi and G. Férey, *J. Am. Chem. Soc.*, 2009, **132**, 1127-1136.
54. Y. Lin, C. Kong and L. Chen, *RSC Adv.*, 2012, **2**, 6417-6419.
55. A. Khutia and C. Janiak, *Dalton Trans.*, 2014, **43**, 1338-1347.
56. S. Couck, J. F. M. Denayer, G. V. Baron, T. Rémy, J. Gascon and F. Kapteijn, *J. Am. Chem. Soc.*, 2009, **131**, 6326-6327.
57. L. Wu, M. Xue, S.-L. Qiu, G. Chaplais, A. Simon-Masseron and J. Patarin, *Microporous Mesoporous Mater.*, 2012, **157**, 75-81.
58. G. E. Cmarik, M. Kim, S. M. Cohen and K. S. Walton, *Langmuir*, 2012, **28**, 15606-15613.
59. Q. Yang, A. D. Wiersum, P. L. Llewellyn, V. Guillerm, C. Serre and G. Maurin, *Chem. Commun.*, 2011, **47**, 9603-9605.
60. Y. Zhao, H. Wu, T. J. Emge, Q. Gong, N. Nijem, Y. J. Chabal, L. Kong, D. C. Langreth, H. Liu, H. Zeng and J. Li, *Chem. Eur. J.*, 2011, **17**, 5101-5109.
61. B. Arstad, H. Fjellvåg, K. Kongshaug, O. Swang and R. Blom, *Adsorption*, 2008, **14**, 755-762.
62. G. Akiyama, R. Matsuda, H. Sato, A. Hori, M. Takata and S. Kitagawa, *Microporous Mesoporous Mater.*, 2012, **157**, 89-93.
63. H. Reinsch, B. Marszalek, J. Wack, J. Senker, B. Gil and N. Stock, *Chem. Commun.*, 2012, **48**, 9486-9488.
64. J. An, S. J. Geib and N. L. Rosi, *J. Am. Chem. Soc.*, 2009, **131**, 8376-8377.
65. J. An and N. L. Rosi, *J. Am. Chem. Soc.*, 2010, **132**, 5578-5579.
66. J. An, S. J. Geib and N. L. Rosi, *J. Am. Chem. Soc.*, 2009, **132**, 38-39.
67. J.-R. Li, Y. Tao, Q. Yu, X.-H. Bu, H. Sakamoto and S. Kitagawa, *Chem. Eur. J.*, 2008, **14**, 2771-2776.
68. Q. Lin, T. Wu, S.-T. Zheng, X. Bu and P. Feng, *J. Am. Chem. Soc.*, 2011, **134**, 784-787.
69. P. Pachfule, R. Das, P. Poddar and R. Banerjee, *Cryst. Growth Des.*, 2010, **10**, 2475-2478.
70. T. Panda, P. Pachfule, Y. Chen, J. Jiang and R. Banerjee, *Chem. Commun.*, 2011, **47**, 2011-2013.
71. J.-B. Lin, W. Xue, J.-P. Zhang and X.-M. Chen, *Chem. Commun.*, 2011, **47**, 926-928.
72. R. Vaidhyanathan, S. S. Iremonger, K. W. Dawson and G. K. H. Shimizu, *Chem. Commun.*, 2009, 5230-5232.
73. J.-B. Lin, J.-P. Zhang and X.-M. Chen, *J. Am. Chem. Soc.*, 2010, **132**, 6654-6656.
74. H. A. Patel, S. Hyun Je, J. Park, D. P. Chen, Y. Jung, C. T. Yavuz and A. Coskun, *Nat. Commun.*, 2013, **4**, 1357.
75. R. Vaidhyanathan, S. S. Iremonger, G. K. H. Shimizu, P. G. Boyd, S. Alavi and T. K. Woo, *Angew. Chem., Int. Ed.*, 2012, **51**, 1826-1829.
76. R. Vaidhyanathan, S. S. Iremonger, G. K. H. Shimizu, P. G. Boyd, S. Alavi and T. K. Woo, *Science*, 2010, **330**, 650-653.
77. B. Zheng, J. Bai, J. Duan, L. Wojtas and M. J. Zaworotko, *J. Am. Chem. Soc.*, 2010, **133**, 748-751.
78. M.-S. Chen, M. Chen, S. Takamizawa, T.-a. Okamura, J. Fan and W.-Y. Sun, *Chem. Commun.*, 2011, **47**, 3787-3789.
79. R. Dawson, D. J. Adams and A. I. Cooper, *Chem. Sci.*, 2011, **2**, 1173-1177.
80. A. Torrisi, R. G. Bell and C. Mellot-Draznieks, *Cryst. Growth Des.*, 2010, **10**, 2839-2841.
81. Q. Yang, S. Vaesen, F. Ragon, A. D. Wiersum, D. Wu, A. Lago, T. Devic, C. Martineau, F. Taulelle, P. L. Llewellyn, H. Jobic, C. Zhong, C. Serre, G. De Weireld and G. Maurin, *Angew. Chem.*, 2013, **125**, 10506-10510.
82. W. Lu, D. Yuan, J. Sculley, D. Zhao, R. Krishna and H.-C. Zhou, *J. Am. Chem. Soc.*, 2011, **133**, 18126-18129.
83. C. Serre, S. Bourrelly, A. Vimont, N. A. Ramsahye, G. Maurin, P. L. Llewellyn, M. Daturi, Y. Filinchuk, O. Leynaud, P. Barnes and G. Férey, *Adv. Mater.*, 2007, **19**, 2246-2251.
84. R. Banerjee, H. Furukawa, D. Britt, C. Knobler, M. O'Keeffe and O. M. Yaghi, *J. Am. Chem. Soc.*, 2009, **131**, 3875-3877.
85. Q. Yang, V. Guillerm, F. Ragon, A. D. Wiersum, P. L. Llewellyn, C. Zhong, T. Devic, C. Serre and G. Maurin, *Chem. Commun.*, 2012, **48**, 9831-9833.
86. Y.-S. Bae, O. K. Farha, J. T. Hupp and R. Q. Snurr, *J. Mater. Chem.*, 2009, **19**, 2131-2134.
87. L. Hou, W.-J. Shi, Y.-Y. Wang, Y. Guo, C. Jin and Q.-Z. Shi, *Chem. Commun.*, 2011, **47**, 5464-5466.
88. Y. Liu, J.-R. Li, W. M. Verdegaal, T.-F. Liu and H.-C. Zhou, *Chem. Eur. J.*, 2013, **19**, 5637-5643.
89. A. Santra, M. S. Lah and P. K. Bharadwaj, *Z. Anorg. Allg. Chem.*, 2014, **640**, 1134-1140.
90. P. Deria, J. E. Mondloch, E. Tylianakis, P. Ghosh, W. Bury, R. Q. Snurr, J. T. Hupp and O. K. Farha, *J. Am. Chem. Soc.*, 2013, **135**, 16801-16804.
91. A. J. Fletcher, E. J. Cussen, T. J. Prior, M. J. Rosseinsky, C. J. Kepert and K. M. Thomas, *J. Am. Chem. Soc.*, 2001, **123**, 10001-10011.
92. J. A. Dunne, M. Rao, S. Sircar, R. J. Gorte and A. L. Myers, *Langmuir*, 1996, **12**, 5896-5904.
93. C. F. Leong, T. B. Faust, P. Turner, P. M. Usov, C. J. Kepert, R. Babarao, A. W. Thornton and D. M. D'Alessandro, *Dalton Trans.*, 2013, **42**, 9831-9839.
94. K. L. Mulfort and J. T. Hupp, *J. Am. Chem. Soc.*, 2007, **129**, 9604-9605.
95. K. L. Mulfort and J. T. Hupp, *Inorg. Chem.*, 2008, **47**, 7936-7938.
96. K. L. Mulfort, T. M. Wilson, M. R. Wasielewski and J. T. Hupp, *Langmuir*, 2008, **25**, 503-508.

97. Y.-S. Bae, B. G. Hauser, O. K. Farha, J. T. Hupp and R. Q. Snurr, *Microporous Mesoporous Mater.*, 2011, **141**, 231-235.
98. H. Jasuja and K. S. Walton, *J. Phys. Chem. C*, 2013, **117**, 7062-7068.
99. H. Jasuja, J. Zang, D. S. Sholl and K. S. Walton, *J. Phys. Chem. C*, 2012, **116**, 23526-23532.
100. S. Henke and R. A. Fischer, *J. Am. Chem. Soc.*, 2011, **133**, 2064-2067.
101. H. Jasuja, Y.-g. Huang and K. S. Walton, *Langmuir*, 2012, **28**, 16874-16880.
102. J. Yang, A. Grzech, F. M. Mulder and T. J. Dingemans, *Chem. Commun.*, 2011, **47**, 5244-5246.
103. T. A. Makal, X. Wang and H.-C. Zhou, *Cryst. Growth Des.*, 2013, **13**, 4760-4768.
104. R. Babarao, C. J. Coghlan, D. Rankine, W. M. Bloch, G. K. Gransbury, H. Sato, S. Kitagawa, C. J. Sumby, M. R. Hill and C. J. Doonan, *Chem. Commun.*, 2014, **50**, 3238-3241.
105. Z. Zhang, S. Xiang, X. Rao, Q. Zheng, F. R. Fronczek, G. Qian and B. Chen, *Chem. Commun.*, 2010, **46**, 7205-7207.